Research Journal of Recent Sciences ISSN 2277-2502
Vol. **15(3),** 101-109, July **(2026)** *Res. J. Recent Sci.*

Steady and Dynamic Analysis of a Porous Land Tapered Slider Bearing Under MHD Couplestress Lubrication

Thippeswamy Gonchigara
Department of Mathematics, Government First Grade College, Harapanahalli, Vijayanagara Dt.-583131, Karnataka, India
thippeswamygonchigara@gmail.com

Available online at: www.isca.in, www.isca.me
Received 14th April 2026, revised 23rd May 2026, accepted 17th June 2026

Abstract

A theoretical investigation is carried out to study the steady and dynamic performance of a porous land tapered slider bearing lubricated with an electrically conducting couple-stress fluid under the influence of an external magnetic field. The governing modified Reynolds equation is formulated by incorporating the effects of porosity, couple-stress fluid behavior, and magnetohydrodynamics. Variations of steady-state pressure distribution, load carrying capacity, dynamic stiffness, and damping coefficient are illustrated graphically. The results indicate that an increase in the permeability parameter leads to a reduction in steady pressure, load capacity, stiffness, and damping characteristics, whereas these performance parameters are significantly enhanced with increasing magnetic field strength and couple-stress fluid parameter.

Keywords: MHD, Couplestress fluid, Land Tapered Slider, Porous, Dynamic stiffness, and Damping Coefficient.

Introduction

The main advantage of porous bearings is that they do not require an external oil supply once the bearing material is impregnated with lubricant during manufacture. In modern machinery and mechanisms, increasing rotational speeds, higher impact loads, and the use of advanced structural materials demand efficient and reliable bearing systems. Porous bearings have proven to be highly effective due to their self-lubricating characteristics, low initial cost, design simplicity, and the ability of the lubricant to penetrate and remain within the pores throughout the bearing's operational life.

The fundamental aspects of hydrodynamic lubrication in porous metal bearings were first studied by Morgan et al.[1,] who identified the critical conditions necessary for effective lubrication. Later, Sanni and Ayomidele[2] investigated hydrodynamic lubrication in porous slider bearings without assuming a small porous facing thickness, providing a more realistic analysis. Prakash and Vij[3] demonstrated that porosity reduces the load-carrying capacity of inclined slider bearings. Since then, numerous studies have explored different configurations and characteristics of porous bearings.

The application of magnetic fields introduces an additional mechanism to control and enhance tribological performance. Since liquid metals are good electrical conductors, the application of electromagnetic forces can significantly improve bearing characteristics. Shukla[4] analyzed magnetohydrodynamic (MHD) effects in composite slider bearings and showed that load-carrying capacity increases with magnetic field strength. Agrawal and Bhatt[5] studied MHD effects in porous inclined slider bearings and found that magnetization of lubricant particles enhance load capacity without increasing friction. Hughes[6] investigated MHD step slider bearings using electrically conducting lubricants and reported substantial improvements in load capacity under both transverse and tangential magnetic fields. Ramanaiah[7] determined the optimal load capacity of parallel plate slider bearings under non-uniform magnetic fields using variational methods. Rodkiewicz and Anwar[8] examined MHD characteristics under arbitrary magnetic field conditions. Lin et al.[9] studied dynamic stiffness and damping, concluding that magnetic fields enhance both properties. Naduvinamani et al.[10] further analyzed static and dynamic characteristics of slider bearings lubricated with couple stress fluids under magnetic field influence.

The theory of couple stress fluids, introduced by Stokes[11], accounts for microstructural effects such as body couples and asymmetric stress tensors, making it suitable for analyzing non-Newtonian lubricants. Several researchers[12–14] have applied this theory to lubrication problems and demonstrated improved bearing performance. Naduvinamani et al.[15] studied MHD effects on circular stepped bearings with couple stress lubricants and observed increased load capacity and prolonged squeeze film time. Hanumagowda[16] analyzed the combined effects of MHD and couple stress on plane slider bearings and reported improvements in both steady-state and dynamic characteristics. Further studies by Hanumagowda and co-authors[17–25] extended this work to land-tapered and porous exponential slider bearings.

However, a detailed study on the steady and dynamic characteristics of MHD porous land-tapered slider bearings lubricated with couple stress fluids has not been sufficiently addressed in the existing tribological literature. Therefore, the present work aims to investigate these characteristics, providing a comprehensive analysis of the combined effects of porosity, magnetohydrodynamics, and couple stress fluid behavior on bearing performance.

Mathematical formulation

Figure-1 shows the geometry of porous land tapered slider bearing of length L lubricated with electrically conducting couple stress fluid. The bearing configuration consists of two surfaces separated by a lubricant film. The x-axis is taken along the lower plane across its length, while the y-axis is taken across the lubricant film. The lower surface is moving with a velocity U in its own plane and has a porous matrix of uniform thickness δ and a squeezing velocity dh/dt, where t is the time in the y-direction.

$$\mu\frac{\partial^2 u}{\partial y^2}-\eta\frac{\partial^4 u}{\partial y^4}-\sigma B_0^2 u=\frac{\partial p}{\partial x}+\sigma E_z B_0 \tag{1}$$

$$\frac{\partial p}{\partial y}=0 \tag{2}$$

$$\frac{\partial u}{\partial x}+\frac{\partial v}{\partial y}=0 \tag{3}$$

$$\int_{y=0}^{h}\left(E_z+B_0 u\right)dy=0 \tag{4}$$

The film thickness for the inclined plane slider beating can be written as

$$h(x,t)=h_m(t)+h_s(x) \tag{5a}$$

$$h_s(x)=\begin{cases} d\left(1-\dfrac{x}{L_1}\right), & 0\le x\le L_1 \\ 0, & L_1\le x\le L \end{cases} \tag{5b}$$

where $h_m(t)$ is the minimum film thickness, d is the difference of steady inlet-outlet thickness.

The relevant boundary conditions are
At the upper surface $y=h$

$$u=0\ \frac{\partial^2 u}{\partial y^2}=0\ v=\frac{\partial h}{\partial t} \tag{6}$$

At the lower surface $y=0$

$$u=U\ \frac{\partial^2 u}{\partial y^2}=0\ v=v^* \tag{7}$$

In the porous matrix, the components of velocity u^* and v^* follows Darcy's law are given as:

$$u^*=-\frac{k}{\mu\left(1-\beta+\dfrac{kdB_0^2}{\mu m}\right)}\left(\frac{\partial p^*}{\partial x}+\sigma E_Z B_0\right), \tag{8}$$

$$v^*=-\frac{k}{\mu(1-\beta)}\frac{\partial p^*}{\partial y}, \tag{9}$$

In the above, the symbols p^* and k represent the pressure distribution and the permeability parameter in the porous region respectively, δ is the porous layer thickness and β is the ratio of microstructure size to pore size $(=(\eta/\mu)/k)$.

The boundary conditions for the pressure p^* in the porous matrix one can consider as

$$\left.\frac{\partial p^*}{\partial y}\right|_{y=0}=0\text{, (Solid blocking)} \tag{10}$$

$$p^*(x,0)=p(x,0).$$
(Continuity of pressure at the interface) (11)

The continuity equation in the porous region is given by

$$\frac{\partial u^*}{\partial x}+\frac{\partial v^*}{\partial y}=0 \tag{12}$$

Using the velocity components u^* and v^* in Equation (12) and integrating once with respect to y over the porous layer thickness with conditions (10) and (11), gives

$$\left.v^*\right|_{y=0}=\frac{kd}{\mu c^2}\frac{\partial}{\partial x}\left(\frac{\partial p^*}{\partial x}+\sigma E_z B_0\right) \tag{13}$$

where $c=\left(1-\beta+\dfrac{k\sigma B_0^2}{\mu m}\right)^{1/2}$

Solving equation (1) using the boundary conditions (6), (7) and the condition (4), the velocity component is expressed as

$$u=-\frac{U}{2}r_1-\frac{h_{m0}^2 h}{2l\mu M_0^2}\frac{\partial p}{\partial x}r_2 \tag{14}$$

where

$$r_1 = r_{11} - r_{12},\; r_2 = r_{13} - r_{14} \text{ for } 4M_0^2 l^2 / h_{m0}^2 < 1 \tag{15a}$$

$$r_1 = r_{21} - r_{22},\; r_2 = r_{23} - r_{24} \text{ for } 4M_0^2 l^2 / h_{m0}^2 = 1 \tag{15b}$$

$$r_1 = r_{31} - r_{32},\; r_2 = r_{33} - r_{34} \text{ for } 4M_0^2 l^2 / h_{m0}^2 > 1 \tag{15c}$$

$M_0 = B_0 h_{m0} \left(\sigma/\mu\right)^{1/2}$ and $\eta/\mu = l^2$

The MHD Reynold's equation for land tapered porous slider bearing profile lubricated with non-Newtonian fluid one can obtained as

$$\frac{\partial}{\partial x}\left\{ f(h,l,M_0)\frac{\partial p}{\partial x}\right\} = 6U\frac{\partial h}{\partial x} + 12\frac{\partial h}{\partial t} \tag{16}$$

where

$$f(h,l,M_0) = \begin{cases} \dfrac{6h_{m0}^2 h^2}{\mu l M_0^2}\left\{ \dfrac{A^2 - B^2}{\dfrac{A^2}{B}\tanh\dfrac{Bh}{2l} - \dfrac{B^2}{A}\tanh\dfrac{Ah}{2l}}\left(1 + \dfrac{kdM^2}{hc^2 h_{m0}}\right) - \dfrac{2l}{h}\right\} & \text{for } 4M_0^2 l^2/h_{m0}^2 < 1 \\ \dfrac{6h_{m0}^2 h^2}{\mu l M_0^2}\left\{ \dfrac{2\left(Cosh\left(h/\sqrt{2}l\right)+1\right)}{3\sqrt{2}Sinh\left(h/\sqrt{2}l\right) - h/l}\left(1 + \dfrac{kdM^2}{hc^2 h_{m0}}\right) - \dfrac{2l}{h}\right\} & \text{for } 4M_0^2 l^2/h_{m0}^2 = 1 \\ \dfrac{6h_{m0}^2 h^2}{\mu l M_0^2}\left\{ \dfrac{M_0\left(CosB_1 h + CoshA_1 h\right)}{h_2\left(A_2 SinB_1 h + B_2 SinhA_1 h\right)}\left(1 + \dfrac{kdM^2}{hc^2 h_{m0}}\right) - \dfrac{2l}{h}\right\} & \text{for } 4M_0^2 l^2/h_{m0}^2 > 1 \end{cases} \tag{17}$$

$$A_2 = \left(B_1 - A_1 Cot\theta\right),\; B_2 = \left(A_1 + B_1 Cot\theta\right)$$

Using the following non-dimensional quantities

$$x^* = \frac{x}{L}, h^*(x^*) = \frac{h(x)}{h_{m0}}, h^*_s(x^*) = \frac{h_s(x)}{h_{m0}}, d^* = \frac{d}{h_{m0}}, P^* = \frac{p^* h_{m0}^2}{\mu UL},$$

$$l^* = \frac{2l}{h_{m0}}, t^* = \frac{t}{h_{m0}} \text{ and } C = \left(1 - \beta + \frac{\psi M_0^2}{m\delta^*}\right)^{1/2} \psi = \frac{k\delta}{h_{m0}^3}$$

in equation (16), the non-dimensional MHD and couplestress Reynolds equation is expressed as

$$\frac{\partial}{\partial x^*}\left\{ f(h^*,l^*,\psi,M_0)\frac{\partial P}{\partial x^*}\right\} = 6\frac{d\left\{d^*(1-x^*)\right\}}{dx^*} + 12\frac{\partial h^*}{\partial t^*} \tag{18}$$

Where

$$h^*(x^*,t^*) = h_m^*(t^*) + h_s^*(x^*) \tag{19a}$$

$$h_s^*(x^*) = \begin{cases} d^*\left(1 - \dfrac{x^*}{L_1^*}\right), & 0 \le x^* \le L_1^* \\ 0, & L_1^* \le x^* \le 1 \end{cases} \tag{19b}$$

$$f^*(h^*,l^*,\psi,M_0) = \begin{cases} \dfrac{12h^{*2}}{l^* M_0^2}\left\{ \dfrac{\left(A^{*2} - B^{*2}\right)}{\dfrac{A^{*2}}{B^*}\tanh\dfrac{B^* h^*}{l^*} - \dfrac{B^{*2}}{A^*}\tanh\dfrac{A^* h^*}{l^*}}\left(1 + \dfrac{\psi M^2}{h^* c^2}\right) - \dfrac{l^*}{h^*}\right\} & \text{for } M_0^2 l^{*2} < 1 \\ \dfrac{12h^{*2}}{l^* M_0^2}\left\{ \dfrac{1 + Cosh\left(\sqrt{2}h^*/l^*\right)}{\left(3/\sqrt{2}\right)Sinh\left(\sqrt{2}h^*/l^*\right) - \left(h^*/l^*\right)}\left(1 + \dfrac{\psi M^2}{h^* c^2}\right) - \dfrac{l^*}{h^*}\right\} & \text{for } M_0^2 l^{*2} = 1 \\ \dfrac{12h^{*2}}{l^* M_0^2}\left\{ \dfrac{M_0\left(CosB_1^* h^* + CoshA_1^* h^*\right)}{A_2^* SinB_1^* h^* + B_2^* SinhA_1^* h^*}\left(1 + \dfrac{\psi M^2}{h^* c^2}\right) - \dfrac{l^*}{h^*}\right\} & \text{for } M_0^2 l^{*2} > 1 \end{cases} \tag{20}$$

$$A^* = \left\{\frac{1 + \left(1 - l^{*2}M_0^2\right)^{1/2}}{2}\right\}^{1/2}, B^* = \left\{\frac{1 - \left(1 - l^{*2}M_0^2\right)^{1/2}}{2}\right\}^{1/2}$$

$$A_1^* = \sqrt{2M_0/l^*}\,Cos\left(\theta^*/2\right),\; B_1^* = \sqrt{2M_0/l^*}\,Sin\left(\theta^*/2\right),$$

$$\theta^* = \tan^{-1}\left(\sqrt{l^{*2}M_0^2 - 1}\right) A_2^* = \left(B_1^* - A_1^* Cot\theta^*\right),$$

$$B_2^* = \left(A_1^* + B_1^* Cot\theta^*\right)$$

Reynolds equation in Region I

$$\frac{\partial}{\partial x^*}\left\{ f(h^*,l^*,\psi,M_0)\frac{\partial P_1}{\partial x^*}\right\} = 6\frac{d\left\{d^*\left(1 - \dfrac{x^*}{L_1^*}\right)\right\}}{dx^*} + 12V \tag{21}$$

Reynolds equation in Region II

$$\frac{\partial}{\partial x^*}\left\{ f(h_m^*,l^*,\psi,M_0)\frac{\partial P_2}{\partial x^*}\right\} = 12V^* \tag{22}$$

Integrating equation (21) and (22) w. r. t. x^*twice, and using the pressure boundary conditions $P_1 = 0$ at $x^* = 0$, $P_1 = P_2$ at x^* = L_1^* and $P_2 = 0$ at $x^* = 1$ gives the MHD and couple stress film pressure

Region I

$$P_1 = 6S_1(0,x^*) + 12V^* S_2(0,x^*) + C_1 S_3(0,x^*)S$$

where

$$S_1(0,x^*) = \int_{x^*=0}^{x^*} \frac{d^*\left(1 - \dfrac{x^*}{L_1^*}\right)}{f^*(h^*,l^*,\psi,M_0)}dx^*, S_2(0,x^*) = \int_{x^*=0}^{x^*} \frac{x^*}{f^*(h^*,l^*,\psi,M_0)}dx^*$$

$$S_3(0,x^*) = \int_{x^*=0}^{x^*} \frac{1}{f^*(h^*,l^*,\psi,M_0)}dx^* \tag{23}$$

Region II

$$P_2 = 12V^* S_4(1,x^*) + C_1 S_5(1,x^*)$$

where

$$S_4(1,x^*) = \int_{x^*=1}^{x^*} \frac{x^*}{f^*(h_m^*,l^*,\psi,M_0)}dx^*, S_5(1,x^*) = \int_{x^*=1}^{x^*} \frac{1}{f^*(h_m^*,l^*,\psi,M_0)}dx^* \tag{24}$$

where $V^* = dh_m^* / dt^*$ is the non-dimensional squeezing velocity, and

The load per unit width is given by

$$w = b\int_0^L p\,dx$$

By letting the minimum film height be constant and letting squeezing velocity be zero, the dimensionless load carrying capacity is

$$W^* = \int_{x^*=0}^{L_1^*} P_1 dx^* + \int_{x^*=L_1^*}^{1} P_2 dx^*$$

$$W^* = 6S_{21}(0, L_1^*) + 12V^* \left\{S_{22}(0, L_1) + S_{23}(L_1, 1)\right\} + C_1 \left\{S_{24}(0, L_1^*) + S_{25}(L_1^*, 1)\right\}$$

Where

$$S_{21}(0, L_1^*) = \int_0^{L_1^*} \int_{x^*=0}^{x^*} \frac{d^*\left(1 - \frac{x^*}{L_1^*}\right)}{f^*(h^*, l^*, \psi, M_0)} dx^* dx^*, \quad S_{22}(0, L_1^*) = \int_0^{L_1^*} \int_{x^*=0}^{x^*} \frac{x^*}{f^*(h^*, l^*, \psi, M_0)} dx^* dx^*$$

$$S_{23}(L_1^*, 1) = \int_{L_1^*}^{1} \int_{x^*=1}^{x^*} \frac{x^*}{f^*(h_m^*, l^*, \psi, M_0)} dx^* dx^*, \quad S_{24}(0, L_1^*) = \int_{x^*=0}^{L_1^*} \int_{x^*=0}^{x^*} \frac{1}{f^*(h^*, l^*, \psi, M_0)} dx^* dx^* \tag{25}$$

$$S_{25}(L_1^*, 1) = \int_{L_1^*}^{1} \int_{x^*=1}^{x^*} \frac{1}{f^*(h_m^*, l^*, \psi, M_0)} dx^* dx^*$$

By letting the minimum film height be constant and letting squeezing velocity be zero in equations (21) and (22), the dimensionless steady film pressure p_s^* and the dimensionless load carrying capacity W_s^* is given by

Region I

$$P_{1s} = 6S_1(0, x^*) + C_{1s}S_3(0, x^*) \tag{26}$$

Region II

$$P_{2s} = C_{1s} \ S_5(1, x^*) \tag{27}$$

$$W_s^* = 6S_{21}(0, L_1^*) + C_{1s} \left\{S_{24}(0, L_1^*) + S_{25}(L_1^*, 1)\right\} \tag{28}$$

$$C_{1s} = -\frac{6S_6(0, L_1^*)}{\left\{S_7(0, L_1^*) - S_8(1, L_1^*)\right\}}$$

where

$$S_6(0, L_1^*) = \int_{x^*=0}^{L_1^*} \frac{d^*\left(1 - \frac{x^*}{L_1^*}\right)}{f^*(h^*, l^*, \psi, M_0)} dx^*, \quad S_7(0, L_1^*) = \int_{x^*=0}^{L_1^*} \frac{1}{f^*(h^*, l^*, \psi, M_0)} dx^*$$

$$S_8(1, L_1^*) = \int_{x^*=1}^{L_1^*} \frac{1}{f^*(h_m^*, l^*, \psi, M_0)} dx^*$$

Differentiating MHD film force partially with respect to dimensionless minimum film thickness and thereafter taking the value under steady state gives the dimensionless linear dynamic stiffness coefficient is given by

$$S_d^* = -\left(\frac{\partial W_s^*}{\partial h_m^*}\right) = -[6S_{26}(0, L_1^*) - 6\left\{\frac{\left(S_7(0, L_1^*) - S_8(1, L_1^*)\right)\left(S_9(0, L_1^*)\right) - \left(S_6(0, L_1^*)\right)\left(S_{10}(0, L_1^*) - S_{11}(1, L_1^*)\right)}{\left(S_7(0, L_1^*) - S_8(1, L_1^*)\right)^2}\right\}$$

$$\times\left(S_{24}(0, L_1^*) + S_{25}(L_1^*, 1)\right) + 6C_{1s}\left(S_{27}(0, L_1^*) + S_{28}(L_1^*, 1)\right)\Big]$$

where

$$S_{26}(0, L_1^*) = \int_{x^*=0}^{L_1^*} \int_{x^*=0}^{x^*} h_s^*(-1) f^{*-2} \frac{\partial f^*(h^*, l^*, \psi, M_0)}{\partial h_m^*} dx^* dx^*, \quad S_9(0, L_1^*) = \int_{x^*=0}^{L_1^*} h_s^*(-1) f^{*-2} \frac{\partial f^*(h^*, l^*, \psi, M_0)}{\partial h_m^*} dx^*$$

$$S_{10}(0, L_1^*) = \int_{x^*=0}^{L_1^*} (-1) f^{*-2} \frac{\partial f^*(h^*, l^*, M_0)}{\partial h_m^*} dx^*, \quad S_{11}(1, L_1^*) = \int_{x^*=1}^{L_1^*} (-1) f^{*-2} \frac{\partial f^*(h_m^*, l^*, \psi, M_0)}{\partial h_m^*} dx^*$$

$$S_{27}(0, L_1^*) = \int_{x^*=0}^{L_1^*} \int_{x^*=0}^{x^*} (-1) f^{*-2} \frac{\partial f^*(h^*, l^*, \psi, M_0)}{\partial h_m^*} dx^* dx^*, \quad S_{28}(L_1^*, 1) = \int_{L_1^*}^{1} \int_{x^*=1}^{x^*} (-1) f^{*-2} \frac{\partial f^*(h_m^*, l^*, \psi, M_0)}{\partial h_m^*} dx^* dx^* \tag{29}$$

Differentiating MHD film force partially with respect to dimensionless squeezing velocity and thereafter taking the value under steady state gives the dimensionless linear dynamic stiffness coefficient is given by

$$D_d^* = -\left(\frac{\partial W^*}{\partial V^*}\right) = -12\left\{S_{22}(0, L_1^*) + S_{23}(L_1^*, 1)\right\} + \left\{\frac{12\left(S_{12}(0, L_1^*) - S_{13}(0, L_1^*)\right)}{\left(S_7(0, L_1^*) - S_8(1, L_1^*)\right)}\right\}\left\{S_{24}(0, L_1^*) + S_{25}(L_1^*, 1)\right\} \tag{30}$$

where

$$S_{12}(0, L_1^*) = \int_{x^*=0}^{L_1^*} \frac{x^*}{f^*(h^*, l^*, \psi, M_0)} dx^*, \quad S_{13}(0, L_1^*) = \int_{x^*=1}^{L_1^*} \frac{x^*}{f^*(h_m^*, l^*, \psi, M_0)} dx^*$$

Results and Discussions

The effect of permeability on MHD bearing lubricated with couple stress fluid is analysed under the steady state condition. The permeability parameter ψ signifies the effect of permeability resulting from the fluid which flows into the porous matrix, signifies the effect of couple stresses resulting from additives added to Newtonian fluid, the Hartmann number H signifies the effect of magnetic field resulting from an externally applied magnetic field. The results of Naduvinamani *et al.*[10] can be recovered as a limiting case with $\psi \rightarrow 0$ for solid case and also Siddaram Patil[10] studied the static and dynamic characteristics of porous MHD plane inclined slider bearing lubricated with couple stress fluid

Steady film pressure: Figure-2 shows the variation of non-dimensional steady film pressure Ps^* with non dimensional coordinate x^*, for different values of Hartmann number M_0. It is observed that, the pressure increases for the increasing values of the Hartmann number M_0 and as x^* value increases the pressure P_s^* increases and reaches its maximum then starts decreasing.

Figure-3 shows the variation of non-dimensional steady film pressure Ps^* with on dimensional coordinate x^*, for different values of couple stress parameter l^*. It is observed that, the presence of couple stresses increases Ps^* in the film as compared to the corresponding Newtonian case and as x^* value increases the pressure P_s^* increases and reaches its maximum then starts decreasing.

Figure-4 depicts the variation of non-dimensional steady film pressure Ps^* with on dimensional coordinate x*, for different values of h_m^*. It is observed that, the pressure increases for the increasing values of the non-dimensional minimum film height h_m^* and as x^* value increases the pressure P_s^* increases and reaches its maximum then starts decreasing.

Figure-5 shows the variation of non-dimensional steady film pressure Ps^* with permeability parameter ψ, for different values of couple stress parameter l^*. It is observed that, as the permeability parameter takes higher values, the pressure starts decreasing. Whereas the effect of permeability is marginal in the presence of magnetic field.

Steady load carrying capacity: Figure-6 shows the variation of non-dimensional steady load carrying capacity W_S^* with the profile parameter d^* different values of the Hartmann number M_0. It is observed that the non dimensional load carrying capacity increases with increasing values of d^* until maximum is obtained, there after decreases with increasing values of d^* at which W_s^* attains maximum value.

Figure-7 shows the variation of non-dimensional steady load carrying capacity W_S^* with the profile parameter d^* for different values of couple stress parameter l^*. It is observed that the non dimensional load carrying capacity increases with increasing values of d^* until maximum is obtained, there after decreases with increasing values of d^* at which W_s^* attains maximum value.

Figure-8 shows the variation of non-dimensional steady load carrying capacity W_S^* with the profile parameter δ, for different values of h_m^*. It is observed that the non dimensional load carrying capacity increases with increasing values of d^* until maximum is obtained, there after decreases with increasing values of d^* at which W_s^* attains maximum value.

Figure-9 shows the variation of non-dimensional steady load carrying capacity W_S with permeability parameter ψ, for different values of couple stress parameter l^*. It is observed that, as the permeability parameter takes higher values, the pressure starts decreasing. Whereas the effect of permeability is marginal in the presence of magnetic field.

Dynamic stiffness: Figure-10 depicts the variation of dynamic stiffness S_d^* with the profile parameter d^* different values of the Hartmann number M_0^*. It is observed that the dynamic stiffness increases with increasing values of δ until maximum is obtained, there after decreases with increasing values of d^*.

Figure-11 depicts the variation of dynamic stiffness S_d^* with the profile parameter d^* different values of the couple stress parameter l^*. It is observed that the dynamic stiffness increases with increasing values of δ until maximum is obtained, there after decreases with increasing values of d^*.

Figure-12 depicts the variation of dynamic stiffness S_d^* with the profile parameter d^* different values of the h_m^*. It is observed that the dynamic stiffness increases with increasing values of d^* until maximum is obtained, there after decreases with increasing values of d^*.

Figure-13 shows the variation of non-dimensional steady load carrying capacity S_d with permeability parameter ψ, for different values of couple stress parameter l^*. It is observed that, as the permeability parameter takes higher values, the pressure starts decreasing. Whereas the effect of permeability is marginal in the presence of magnetic field.

Damping coefficient: Figure-14 depicts the variation of damping coefficient D_d^* with the profile parameter δ different values of the Hartmann number M_0. It is observed that the damping coefficient decreases with increasing values of δ,

Figure-15 depicts the variation of damping coefficient D_d^* with the profile parameter d^* different values of the couple stress parameter l^*. It is observed that the damping coefficient decreases with increasing values of d^*.

Figure-16 depicts the variation of damping coefficient D_d^* with the profile parameter d* different values of h_m^*. It is observed that the damping coefficient decreases with increasing values of d^*.

Figure-17 shows the variation of non-dimensional steady load carrying capacity D_d^* with permeability parameter ψ, for different values of couple stress parameter l. It is observed that, as the permeability parameter takes higher values, the pressure starts decreasing. Whereas the effect of permeability is marginal in the presence of magnetic field.

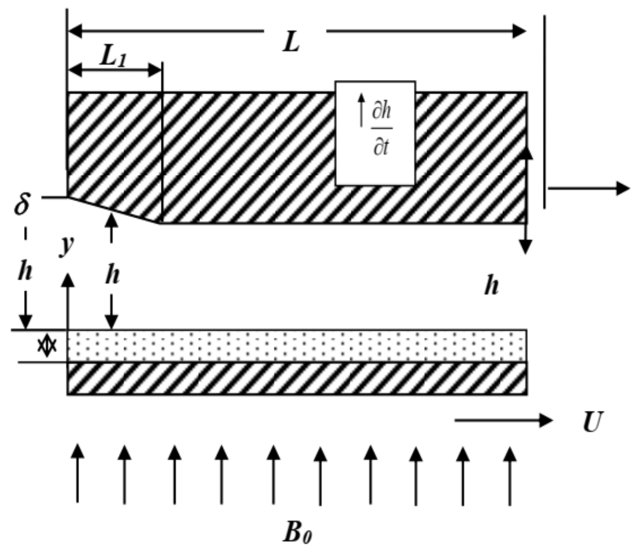

Figure-1: Schematic diagrams of porous land tapered slider bearing.

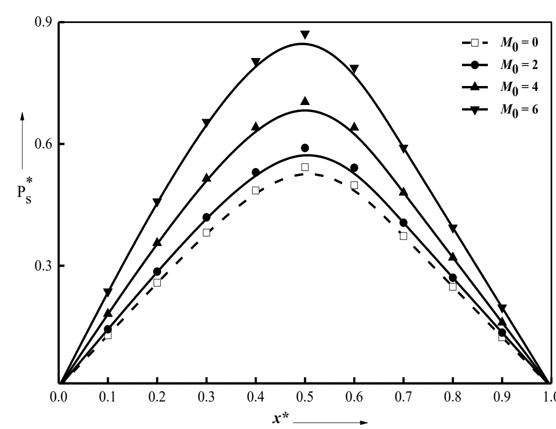

Figure-2: Variation of steady film pressure P_S^* with x^* for different values of M_0withh_m^*= 0.8, l^* = 0.3, ψ = 0.001, α = 0.6, δ = 0.6, β = 0.1, m = 0.06.

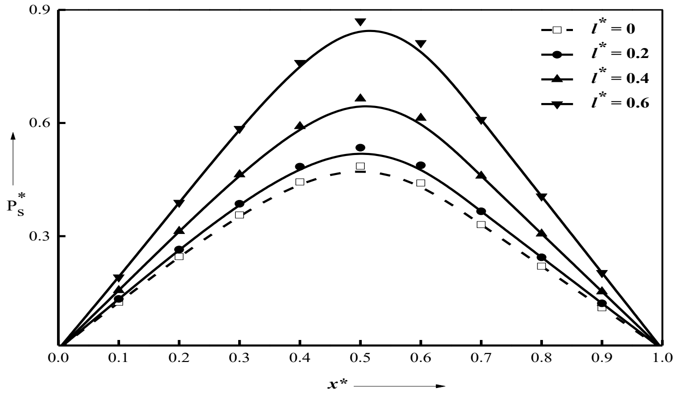

Figure-3: Variation of steady film pressure P_S^* with x^* for different values of l^* with h_m^*= 0.8, M_0 = 2, ψ= 0.001, α = 0.6, δ= 0.6, β= 0.1, m = 0.06.

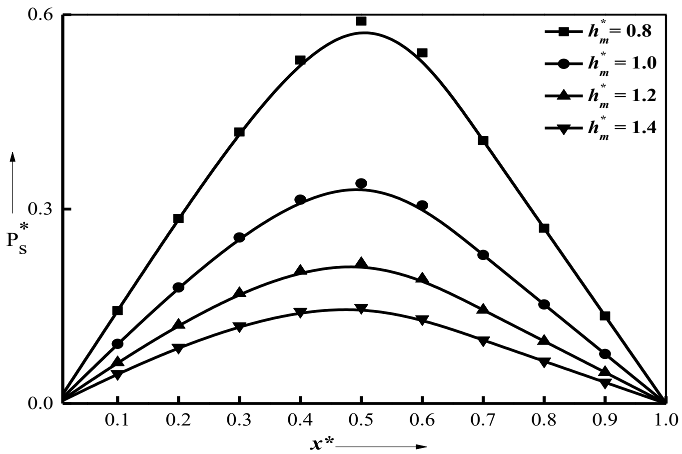

Figure-4: Variation of steady film pressure P_S^* with x^* for different values of h_m^* with l^* = 0.3, M_0 = 2, = 0.001, α= 0.6, δ= 0.6, β= 0.1, m = 0.06.

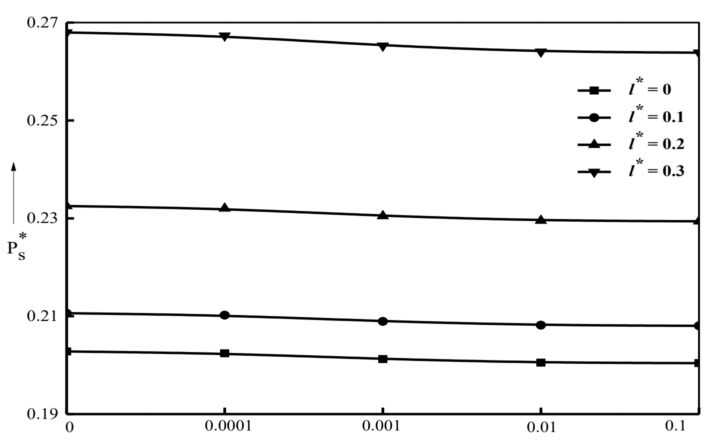

Figure-5: Variation of steady film pressure P_S^* with ψ for different values of l^* with h_m^* = 0.8, M_0 = 1, α= 0.6, δ= 0.6, β = 0.1, m = 0.06, x^*= 0.5.

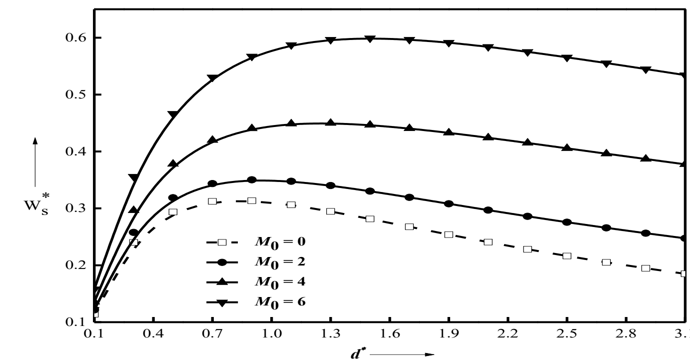

Figure-6: Variation of steady load carrying capacity W_S^* with d^* for different values of M_0 with h_m^* = 0.8, l^* = 0.3,   = 0.001, α = 0.6, β = 0.1, m = 0.06.

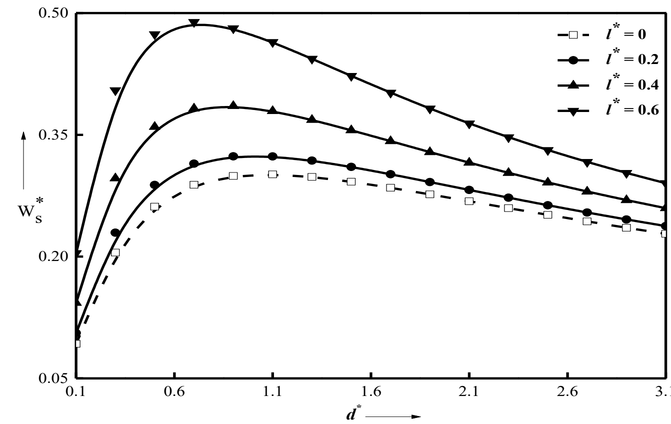

Figure-7: Variation of steady load carrying capacity W_S^* with d*for different values of l^* with h_m^* = 0.8, M_0 = 2, ψ= 0.001, α= 0.6, β= 0.1, m = 0.06.

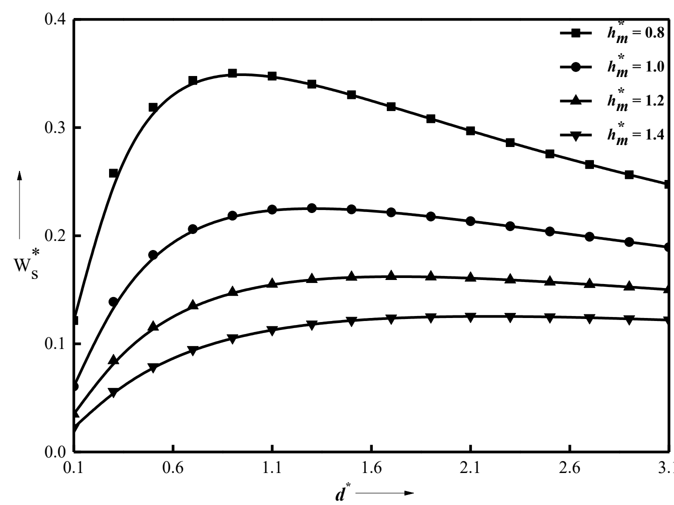

Figure-8: Variation of steady load carrying capacity W_S^* with d* for different values of h_m^* with l^* = 0.3, M_0 = 2, ψ = 0.001, α = 0.6, β = 0.1, m = 0.06.

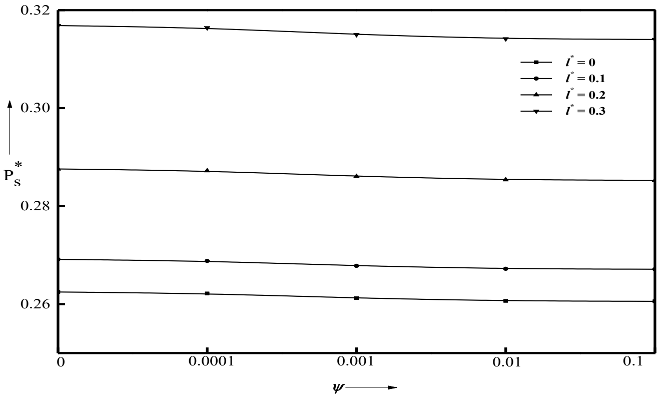

Figure-9: Variation of steady load carrying capacity W_S^* with $\psi$for different values of l^* with h_m^* = 0.8, M_0 = 1, α= 0.6, δ= 0.6, β= 0.1, m = 0.06.

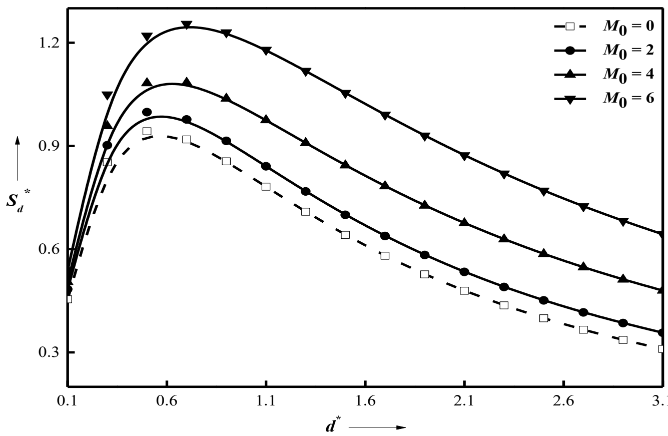

Figure-10: Variation of dynamic stiffness coefficient S_d^* with d^* for different values of M_0 with h_m^* = 0.8, l^* = 0.3, ψ= 0.001, α = 0.6, β = 0.1, m = 0.06.

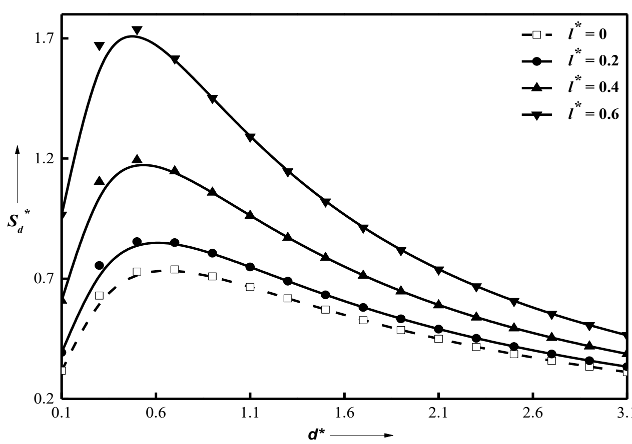

Figure-11: Variation of dynamic stiffness coefficient S_d^* with d^* for different values l^* with h_m^* = 0.8, M_0 = 2,   = 0.001, α = 0.6, β = 0.1, m = 0.06.

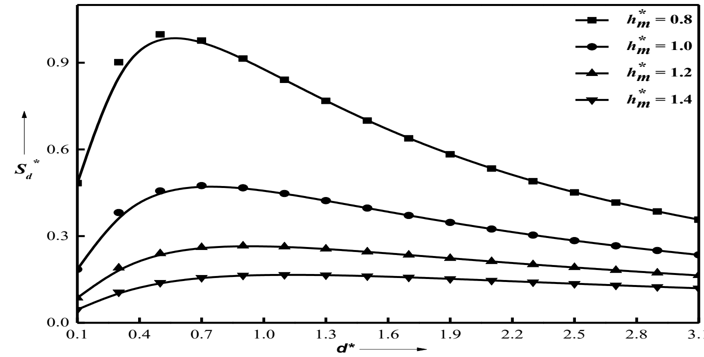

Figure-12: Variation of dynamic stiffness coefficient S_d^* with d^* for different values of $h_m^*$with l^* = 0.3, M_0 = 2,   = 0.001, α = 0.6, β = 0.1, m = 0.06.

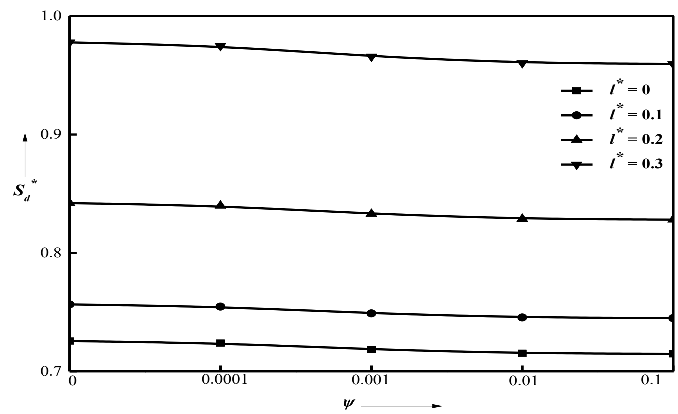

Figure-13: Variation of dynamic stiffness coefficient S_d^* with ψ for different values l^* with h_m^* = 0.8, M_0 = 1, α = 0.6, δ = 0.6, β = 0.1, m = 0.06.

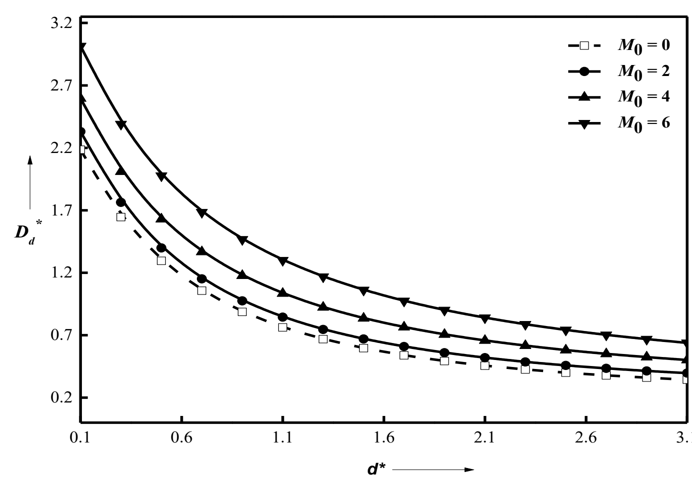

Figure-14: Variation of dynamic damping coefficient D_d^* with d^* for different values of M_0 with h_m^* = 0.8, l^* = 0.3,   = 0.001, α = 0.6, β = 0.1, m = 0.06.

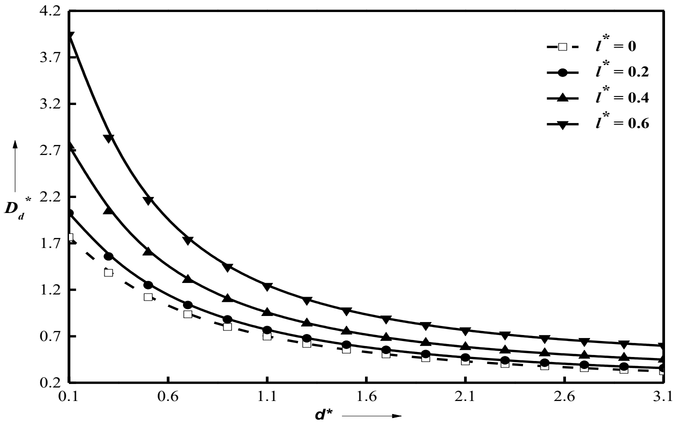

Figure 15: Variation of dynamic damping coefficient D_d^* with d^* for different values of l^* with $h_m^* = 0.8$, $M_0 = 2$, = 0.001, $\alpha = 0.6$, $\beta = 0.1$, $m = 0.06$.

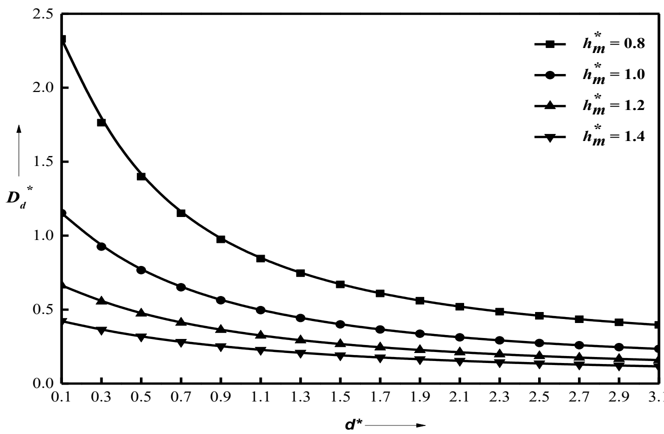

Figure-16: Variation of dynamic damping coefficient D_d^* with d^* for different values of $h_m^*$with $l^* = 0.3$, $M_0 = 2$, = 0.001, $\alpha = 0.6$, $\beta = 0.1$, $m = 0.06$.

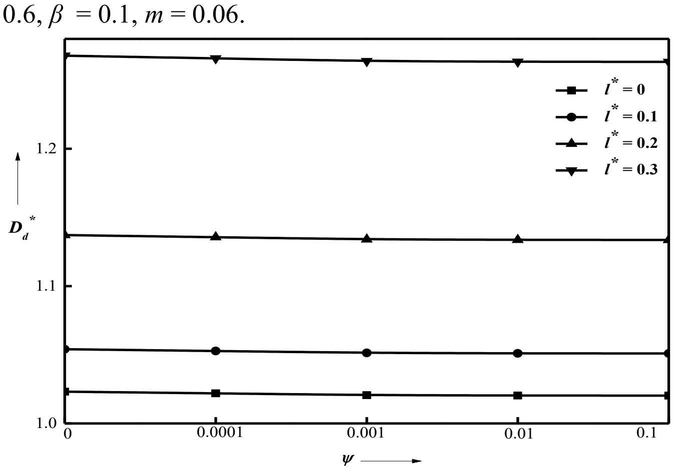

Figure-17: Variation of dynamic damping coefficient D_d^* with ψ for different values of l^* with $h_m^* = 0.8$, $M_0 = 1$, $\alpha = 0.6$, $\delta = 0.6$, $\beta = 0.1$, $m = 0.06$.

Conclusion

The effect of MHD on couple stress fluid lubricated inclined land tapered slider bearing with porous is analyzed by deriving the modified Reynolds equation using Stokes micro-continuum theory and magneto-hydrodynamic thin film lubrication theory. The results show that for the porous land tapered slider bearing, the non-dimensional steady film pressure, non-dimensional steady load carrying capacity, dynamic stiffness, and damping coefficient increase with increasing values of the Hartmann number M_0 and the couple stress parameter l^**compared to the nonmagnetic case* ($M_0 = 0$) *and Newtonian case* ($l^*=0$). These parameters, except the damping coefficient which decreases, increase with increasing values of d^* *until a maximum is reached, after which they decrease with further increases in* d^*. Additionally, the non-dimensional steady film pressure, load carrying capacity, dynamic stiffness, and damping coefficient decrease with increasing values of the non-dimensional minimum film height $h_{m.}^*$. Similarly, the non-dimensional steady film pressure, load carrying capacity, and dynamic stiffness decrease with increasing values of the porous parameter ψ .

References

1. Morgan, V. T., & Cameron, A. (1957). Mechanism of lubrication in porous metal bearings. In *Proceedings of the Conference on Lubrication and Wear*, 89,151–157.

2. Sanni, S. A., & Ayomidele, I. O. (1991). Hydrodynamic lubrication of a porous slider: Limitations of the simplifying assumption of a small porous facing thickness. *Wear,* 147(1), 1–7.

3. Prakash, J., & Vij, S. K. (1974). Squeeze films in porous bearings. *Wear,* 27(3), 359–366.

4. Shukla, J. B. (1964). The magnetohydrodynamic composite slider bearing. *Wear,* 7(5), 460–465.

5. Agrawal, V. K., & Bhatt, S. B. (1980). Porous pivoted slider bearings lubricated with a micropolar fluid. *Wear,* 61(1), 1–8.

6. Hughes, W. F. (1963). The magnetohydrodynamic finite step slider bearing. *Journal of Basic Engineering,* 85, 129–136.

7. Ramanaiah, G. (1963). Optimal load carrying capacity of a parallel plate slider bearing. *Japanese Journal of Applied Physics,* 6, 797–801.

8. Rodkiewicz, C. M., & Anwar, M. I. (1972). Solution for MHD slider bearing with arbitrary magnetic field. *ASME Journal of Lubrication Technology,* 94, 288–290.

9. Lin, J. R., Hung, C. R., Hsu, C. H., & Lai, C. (2009). Dynamic stiffness and damping characteristics of one-dimensional magnetohydrodynamic inclined-plane slider bearings. *Proceedings of the Institution of Mechanical*

Engineers, Part J: Journal of Engineering Tribology, 223(2), 211–219.

10. Naduvinamani, N. B., Siddangouda, A., & Siddharam, P. (2017). A comparative study of static and dynamic characteristics of parabolic and plane inclined slider bearings lubricated with MHD couple stress fluids. *Tribology Transactions, 60*(1), 1–11.

11. Stokes, V. K. (1966). Couple stresses in fluids. *Physics of Fluids,* 9, 1709–1715.

12. Gupta, R. S., & Sharma, L. G. (1988). Analysis of couple stress lubricant in hydrostatic thrust bearing. *Wear, 125*(3), 257–269.

13. Rodkiewicz, C. M., & Anwar, M. I. (1972). Effects of step-type magnetic field in slider bearing. *Wear, 21*(2), 223–229.

14. Lin, J. R., & Lu, Y. M. (2004). Steady-state performance of wide parabolic-shaped slider bearings with a couple stress fluid. *Journal of Marine Science and Technology, 12*(4), 2–10.

15. Naduvinamani, N. B., Fathima, S. T., & Hanumagowda, B. N. (2011). Magnetohydrodynamic couple stress squeeze film lubrication of circular stepped plates. *Proceedings of the Institution of Mechanical Engineers, Part J: Journal of Engineering Tribology,* 225(3), 111–119.

16. Naganagowda, H. B. (2016). Effect of magnetohydrodynamics and couple stress on steady and dynamic characteristics of plane slider bearing. *Tribology Online,* 11(1), 40–49.

17. Hanumagowda, B. N., Gonchigara, T., Kumar, J. S., & Shivakumar, H. M. (2017). Steady and dynamic characteristics of MHD land-tapered slider bearing using Stokes' couple stress model. *International Journal of Pure and Applied Mathematics,* 113, 325–333.

18. Hanumagowda, B. N., Gonchigara, T., Kumar, J. S., & Shivakumar, H. M. (2018). Study of effect of magnetohydrodynamics and couple stress on steady and dynamic characteristics of porous exponential slider bearings. *Journal of Physics: Conference Series,* 1000(1), Article 012091.

19. Hanumagowda, B. N., & Salma, A. (2018). Study of squeeze film performance with MHD and couple stress between curved annular plates. *International Journal of Research and Analytical Reviews,* 5(3), 669–676.

20. Ayyappa, G. H., Hanumagowda, B. N., Siddharam, P., & Jagadish, P. (2020). Influence of magnetic field on a curved circular plate and flat plate lubricated with non-Newtonian fluid. *Journal of Physics: Conference Series,* 1473(1), 1–12.

21. Naduvinamani, N. B., Hiremath, P. S., & Gurubasawaraj, G. (2001). Squeeze film lubrication of a short porous journal bearing with a couple stress fluid. *Industrial Lubrication and Tribology,* 53(2), 73–77.

22. Gonchigara, T. (2025). Analysis of steady and dynamic MHD performance of circular sine-film thrust bearing with couple stress fluid under surface roughness. *International Journal of Engineering Sciences and Management,* 14(4), 119-132.

23. Gonchigara, T. (2026). Effect of roughness on steady and dynamic characteristics of pivot slider bearing with MHD and couple stress fluid. *International Journal of Scientific and Applied Mathematics,* 11(2), 24–38.

24. Ayyappa, G. H., Hanumagowda, B. N., Siddharam, P., Siddangouda, & Jagadish, P. (2019). Effect of MHD on pivoted curved slider bearing lubricated with non-Newtonian fluid. *IOSR Journal of Engineering, 9*(3).

25. Ayyappa, G. H., Hanumagowda, B. N., Siddharam, P., & Jagadish, P. (2019). Theoretical analysis of MHD effects on curved circular plate and rough flat plate with non-Newtonian fluid. *International Journal of Research and Analytical Reviews,* 6(2), 105-114.